Novel Heme Ligand Displacement by CO in the Soluble Hemophore HasA and Its Proximal Ligand Mutants: Implications for Heme Uptake and Release[†]

Gudrun S. Lukat-Rodgers,[‡] Kenton R. Rodgers,*[,‡] Celia Caillet-Saguy,[§] Nadia Izadi-Pruneyre,[§] and Anne Lecroisey[§]

Department of Chemistry, Biochemistry, and Molecular Biology, North Dakota State University, 1231 Albrecht Avenue, Fargo, North Dakota 58105-5516, and Unité de Résonance Magnétique Nucléaire des Biomolécules, CNRS URA 2185, Institut Pasteur, Paris, France

Received September 26, 2007; Revised Manuscript Received December 13, 2007

ABSTRACT: $HasA_{SM}$, a hemophore secreted by the Gram-negative bacteria *Serratia marcescens*, extracts heme from host hemoproteins and shuttles it to $HasR_{SM}$, a specific hemophore outer membrane receptor. Heme iron in $HasA_{SM}$ is in a six-coordinate ferric state. It is linked to the protein by the heretofore uncommon axial ligand set, His32 and Tyr75. A third residue of the heme pocket, His83, plays a crucial role in heme ligation through hydrogen bonding to Tyr75. The vibrational frequencies of coordinated carbon monoxide constitute a sensitive probe of trans ligand field, FeCO structure, and electrostatic landscape of the distal heme pockets of heme proteins. In this study, carbonyl complexes of wild-type (WT) $HasA_{SM}$ and its heme pocket mutants His32Ala, Tyr75Ala, and His83Ala were characterized by resonance Raman spectroscopy. The CO complexes of WT $HasA_{SM}$, $HasA_{SM}$(His32Ala), and $HasA_{SM}$-(His83Ala) exhibit similar spectral features and fall above the line that correlates ν_{Fe-CO} and ν_{C-O} for proteins having a proximal imidazole ligand. This suggests that the proximal ligand field in these CO adducts is weaker than that for heme-CO proteins bearing a histidine axial ligand. In contrast, the CO complex of $HasA_{SM}$(Tyr75Ala) has resonance Raman signatures consistent with ImH-Fe-CO ligation. These results reveal that in WT $HasA_{SM}$, the axial ImH side chain of His32 is displaced by CO. This is in contrast to other heme proteins known to have the His/Tyr axial ligand set, wherein the phenolic side chain of the Tyr ligand dissociates upon CO addition. The displacement of His32 and its stabilization in an unbound state is postulated to be relevant to heme uptake and/or release.

Despite its abundance in the Earth's crust, iron is not readily bioavailable under most physiological conditions. It is nonetheless essential for most organisms, including bacteria. Accordingly, bacteria have developed several iron-scavenging mechanisms to assimilate sufficient amounts of iron to survive. One system developed by some Gram-negative pathogens to acquire iron from their hosts involves secretion of a small protein hemophore known as HasA. The *has* (heme acquisition system) operon encodes for the hemophore HasA (*1*), the outer membrane receptor HasR, the inner membrane ABC protein HasD, a membrane fusion protein HasE, and a TonB homologue, HasB (*1*, *2*). Together with an outer membrane protein HasF, HasD and HasE constitute the specific ABC exporter necessary for the secretion of HasA (*1*, *3*, *4*). The function of the hemophores is to capture heme, either from solution or from heme-containing proteins, and to deliver it to the hemophore-specific receptor, HasR. Heme transport through the receptor is HasB dependent and energetically driven by a proton gradient across the inner membrane.

HasA hemophores have been found in *Serratia marcescens* (*1*, *5*), *Pseudomonas aeruginosa* (*5*, *6*), *Yersinia pestis* (*7*), *Pseudonomas fluorescens* (*8*), *Yersinia enterolitica* (Wandersman, C., personal communication), *Yersinia pseudotuberculosis* (Wandersman, C., personal communication), and *Erwinia carotorova* (*9*). They form an independent family of heme binding proteins having no sequence homology to other proteins. The HasA from *Serratia marcescens* ($HasA_{SM}$)[1] is a monomeric, 19 kDa protein that binds one *b*-type heme with a very high affinity ($K_d = 1.9 \times 10^{-11}$) (*10*). It is also isolated as a heme cross-linked domain-swapped dimer in which the heme/HasA ratio is maintained at 1:1 and the heme cross-links the N- and C-terminal domains of separate protein molecules (*11*). It is able to extract heme from various heme binding proteins having lower heme affinities, such as hemoglobin and heme-loaded albumin (*1*, *3*). The crystal structure of holo-$HasA_{SM}$ reveals an $\alpha\beta$ fold that harbors heme in a loop-rich region at the interface between α and β motifs and axial imidazole and phenolate heme ligands provided by His32 and Tyr75. The ImH side chain of the nearby His83 serves as a hydrogen bond acceptor to stabilize the phenolate ligand of Tyr75 (*10*). Although coordination of Tyr to hemes is becoming more widely recognized, His/Tyr coordination is rare. This pair is only found in a few

[†] This work was supported by NIH-NIAID 1R15AI072719-01 (K.R.R.).

* Corresponding author. E-mail: kent.rodgers@ndsu.edu; tel.: (701) 231-8746; fax: (701) 231-8831.

[‡] North Dakota State University.

[§] Institut Pasteur.

[1] Abbreviations: 5c, five coordinate; 6c, six coordinate; BSA, bovine serum albumin; Fe(PPIX), iron protoporphyrin IX; Hb, hemoglobin; HO, heme oxygenase; hHO-1, human heme oxygenase-1; HS, high-spin; LS, low-spin; Mb, myoglobin; p22HBP, heme binding protein isolated from mammalian liver; rR, resonance Raman; SHE, standard hydrogen electrode; $HasA_{SM}$, HasA hemophore from *Serratia marcescens*; TPP, tetraphenylporphyrin; WT, wild-type.

10.1021/bi7019518 CCC: $40.75
Published on Web 01/19/2008

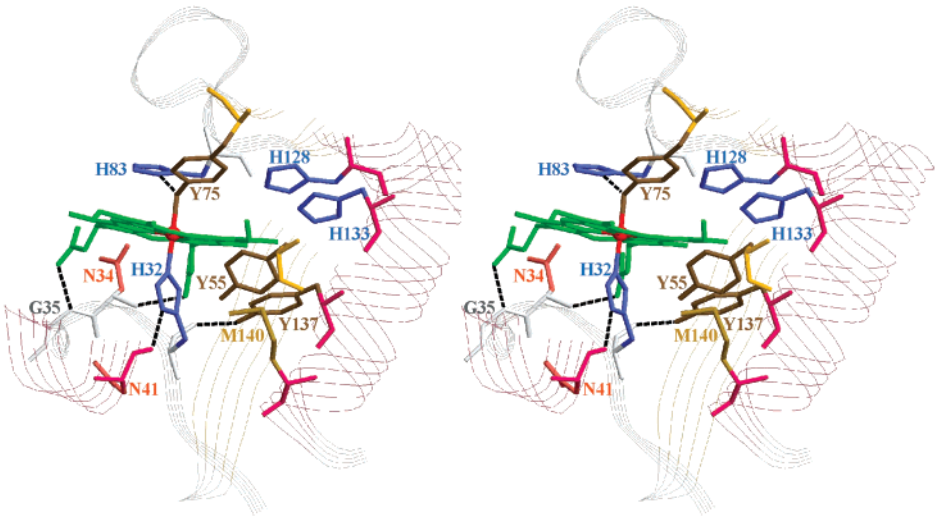

FIGURE 1: Heme environment as observed in the crystal structure of $HasA_{SM}$. Key residues to note are Tyr75, His32, His83, Tyr137, Gly35, Asn41, and Asn34. Thick dashed lines indicate hydrogen bonds, as identified by heavy atom distances from the crystal structure (pdb code: 1DK0).

proteins, in some specific states, including reduced cytochrome *c* maturation protein CcmE (*12*), oxidized cytochrome cd_1 nitrite reductase (*13*), hemoglobin M Saskatoon (*14*), some invertebrate hemoglobins (*15*−*17*), and some ferric myoglobin mutants at neutral and alkaline pH (*18*, *19*). The axial tyrosinate ligand and the solvent-exposed nature of the bound heme are two contributing factors to the exceedingly low reduction potential of −550 mV versus SHE for WT $HasA_{SM}$. This is the most negative potential reported to date for any Fe(III)|Fe(II) couple in a heme protein (*10*, *20*). The heme environment of ferric $HasA_{SM}$, as determined by X-ray crystallography, is illustrated in Figure 1.

A single axial ligand, including the normal H-bond partner of Tyr75, His83, appears to be sufficient for heme binding, as the double mutants $HasA_{SM}$(Y75A/H83A), $HasA_{SM}$(Y75A/H32A), and $HasA_{SM}$(H32A/H83A) bind heme with respectable affinities (K_d values range from 1.7×10^{-5} to 6.3×10^{-7}). Only the triple heme pocket mutant $HasA_{SM}$(Y75A/H32A/H83A) shows no detectable uptake of heme (*21*, *22*). While any one of the heme pocket ligands will facilitate heme binding, the extraordinarily high affinity of $HasA_{SM}$ for ferric heme requires the axially coordinated Tyr75 and its hydrogen bond partner His83 acting in concert to stabilize the heme/$HasA_{SM}$ complex (*21*). Indeed, as shown by ITC, the affinity of $HasA_{SM}$(H32A) for heme is very similar to that of the WT protein ($K_d = 1.0 \times 10^{-10}$), as the synergistic Tyr75 and His83 residues are present in both constructs. On the other hand, the $HasA_{SM}$(Y75A) and $HasA_{SM}$(H83A) mutants have slightly diminished K_d values of 7.7×10^{-9} and 5.0×10^{-9}, respectively, due ostensibly to breaking of the Tyr75-His83 synergy.

Exogenous ligand complexes have long been used to analyze the heme binding sites in hemoproteins. The CO complex of heme has proven to be a particularly sensitive means of probing the coordination and electrostatic character of its protein environment. The C-O and Fe-C stretching frequencies reflect the extent of FeCO backbonding, which is sensitive to FeCO geometry and electrostatic landscape of the distal heme pocket. The position of a heme carbonyl complex on the ν_{Fe-CO} versus ν_{C-O} correlation plot provides useful insight into the distal electrostatic landscape and the σ donor strength of the trans ligand (*23*−*25*). Here, we examine the CO adducts of WT holo$HasA_{SM}$ and three of its heme pocket mutants to assess their axial ligation states. We determine which heme ligand is most readily replaced by the exogenous CO ligand and discuss the implications of these results for partially liganded intermediate states that must occur along the heme binding and release coordinates.

MATERIALS AND METHODS

Protein Expression and Purification. The singly mutated *hasA* genes used in this study, $HasA_{SM}$(H32A), $HasA_{SM}$(Y75A), and $HasA_{SM}$(H83A), were constructed by in vitro site directed mutagenesis (*22*). The WT and mutant $HasA_{SM}$ proteins were obtained from the supernatants of *Escherichia coli* strain Pop3(pSYC34PAM) grown in M9 minimal medium at 30 °C. The proteins were isolated and purified as described previously (*10*, *21*).

Preparation of the holo$HasA_{SM}$s. The $HasA_{SM}$ proteins were isolated as apoproteins. They had a negligible heme content, as judged by the absorbance of their wavelengths for maximum B-band absorbance. Holo$HasA_{SM}$ proteins were generated by titration of the apoproteins with a freshly prepared solution of hemin (*21*) to a heme/$HasA_{SM}$ ratio of ∼1.2:1. Excess heme was separated by gel filtration chromatography (20 mM phosphate buffer, pH 7) to obtain pure heme-loaded $HasA_{SM}$ (hereinafter written as $HasA_{SM}$).

Ferrous CO Complexes. Protein solutions of WT $HasA_{SM}$, $HasA_{SM}$(H32A), and $HasA_{SM}$(H83A) were flushed with carbon monoxide for 20 min immediately prior to the addition of sodium dithionite. A 30−50-fold excess of reducing equivalents was added to the samples by anaerobic transfer of a stock sodium dithionite solution, which was buffered at the appropriate pH. Samples of the corresponding ^{13}CO complexes were prepared by placing an N_2-equilibrated $HasA_{SM}$ solution under 1 atm of ^{13}CO (99 atom % ^{13}C and 10 atom % ^{18}O), followed by reduction, as described for the natural abundance samples. The $HasA_{SM}$(Y75A) mutant was readily reduced by a 2-fold excess of sodium dithionite. Addition of CO or ^{13}CO to ferrous $HasA_{SM}$(Y75A) yielded the respective CO adducts.

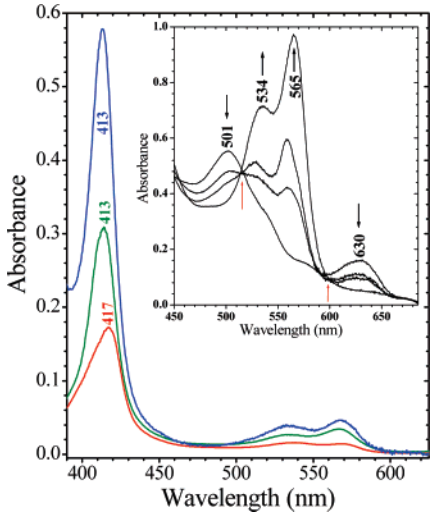

FIGURE 2: Visible spectra of WT $HasA_{SM}$-CO (blue), $HasA_{SM}$-(H32A)-CO (green), and $HasA_{SM}$(Y75A)-CO (red). Reaction of $HasA_{SM}$(H83A) with sodium dithionite and CO was monitored by visible spectroscopy and is shown in the inset. Red arrows below the spectra mark isosbestic points. The black arrows indicate the directions of absorbance changes as the CO complex forms.

Resonance Raman Spectroscopy. Resonance Raman (rR) spectra were recorded from 40 to 100 μM $HasA_{SM}$ solutions, which were contained in 5 mm NMR tubes spinning at ~20 Hz. The Raman excitation was accomplished with either 413.1 nm emission from a Kr^+ laser (3−8 mW) or 441.6 nm emission from a HeCd laser (10−15 mW). UV−vis absorbance spectra were recorded before and after the rR experiments to ensure that the samples had not been irreversibly altered by exposure to the laser beam. No spectral artifacts attributable to laser-induced sample damage were observed. Spectra were recorded at ambient temperature using a 135° back-scattering geometry with the laser beam focused to a line on the spinning NMR tube. Scattered light was collected with an *f*1 lens and filtered with a holographic notch filter to attenuate Rayleigh scattered light. The polarization of the scattered light was then scrambled, and the spot image was *f*-matched to a 0.63 m spectrograph fitted with a 2400 groove/mm grating and a liquid N_2 cooled CCD camera. The spectrometer was calibrated using the Raman bands of toluene, DMF, acetone, and d_6-DMSO as external frequency standards.

Reduction Potentials. Cyclic voltammetry was performed as previously described, using a pyrolytic graphite permselective membrane electrode modified with polylysine to increase the electron transfer rate (*10*, *26*). Potentials are reported versus the standard hydrogen electrode (SHE).

RESULTS

WT $HasA_{SM}$-CO. In the absence of CO, WT $HasA_{SM}$ could not be completely reduced, consistent with its very low reduction potential of −550 mV versus SHE (*10*). Thus, the ferrous $HasA_{SM}$-CO adduct was generated by equilibration of the ferric protein with CO followed by anaerobic transfer of buffered sodium dithionite solution. The UV−vis absorbance spectrum of WT $HasA_{SM}$-CO shows its B-band maximum at 413 nm and its Q-bands at 535 and 568 nm (Figure 2). Table 1 compares these values to those of heme carbonyls in the $HasA_{SM}$ mutants and in proteins whose ferric hemes have either Tyr or Tyr/His axial ligands. It should be noted that upon reduction, the Tyr^- ligand is replaced by axial histidine coordination in the mutant Hbs (*27*). Subsequent formation of the respective HbM-CO complexes and the CO complexes of the analogous Mb mutants maintain His residues as their proximal heme ligands (*18*, *19*, *27*). In these cases, as for other CO adducts having axial histidine ligands, the B-band is observed near 420 nm with Q-bands at 538 and 568 nm (*28*). The higher-energy B-band of WT $HasA_{SM}$-CO (413 nm) thus suggests a proximal environment distinct from those having an axial histidine ligand (420 nm).

The ν_{Fe-CO} and ν_{C-O} Raman bands have been assigned by ^{13}CO substitution as shown in Figure 3. When WT $HasA_{SM}$-CO is labeled with ^{13}CO, the ν_{Fe-CO} frequency shifts from 532 to 523 cm^{-1}, and the ν_{C-O} frequency shifts from 1953 to 1905 cm^{-1}. These two bond stretching frequencies place WT $HasA_{SM}$ considerably above the ImH-Fe-CO line on the ν_{Fe-CO}/ν_{C-O} correlation plot for proteins having proximal His ligands (Figure 4) and very close to human HO-1(H25Y). This position is consistent with the proximal Fe-L bond in WT $HasA_{SM}$-CO being weaker than the proximal Fe-His counterpart, suggesting that WT $HasA_{SM}$-CO contains either a weak proximal Fe(II)-O bond (i.e., Fe(II)-Tyr, Fe(II)-OH_2, or Fe(II)-OH) or no proximal ligand at all.

The breadth, intensity, and isotope sensitivity of the Fe-CO stretching band in Figure 3A warrant some comment. As is apparent from inspection of the natural abundance spectrum (labeled ^{12}CO), the ν_{Fe-CO} band lies among multiple overlapping bands. Furthermore, as seen in the low-frequency difference spectrum, the ν_{Fe-CO} band itself is somewhat broad. This breadth is attributed to flexibility in the heme pocket, which makes multiple states of the bound CO accessible under the ambient conditions of the experiment. The spectrum of the ^{13}CO isotopologue is broader still. The ^{13}CO used in this study was not normalized with respect to ^{18}O. Thus, the increased breadth in the ν_{Fe-CO} band is attributable to the ~10% $^{13}C^{18}O$ present in the ^{13}CO. Asymmetry in the ν_{Fe-CO} and ν_{C-O} difference features throughout this study are also a consequence of the isotopic composition of the ^{13}CO.

The ν_{Fe-CO} band in the Soret excited rR spectrum of catalase-CO has been reported to be more intense than the totally symmetric ν_7 band (*29*). This signature was correlated with the anionic character of the proximal Tyr, whose coordination to heme iron is stabilized by H-bonding to a His residue. It is noteworthy that none of the ν_{Fe-CO} bands in this study are more intense than ν_7, suggesting that none of the $HasA_{SM}$-CO complexes have proximal tyrosinate ligands. The isotope sensitivity of the ν_{Fe-CO} frequency is 2−3 times that of typical heme carbonyl complexes. Assignments of the frequencies for WT $HasA_{SM}$-CO in Figure 3A must be considered approximate due to the overlapping bands in this region of the spectrum and the breadth of the ν_{Fe-CO} band. However, frequency assignments in the (H32A), (H83A), and (Y75A) mutants are all clear, and their ^{13}CO isotope shifts are all 6−7 cm^{-1}, which is approximately double the typical shift and nearly exactly the shift calculated for a two-body, Fe-CO (μ = 19.1) oscillator. Thus, the increased isotope sensitivities in these complexes are attributed to their having relatively weak proximal Fe-L bonds.

Table 1: UV−vis Absorbance Maxima for Comparison of Ferrous Heme Carbonyl Complexes Having Proximal Tyrosine Ligands with Those Having Proximal Histidine Ligands[a]

proteins	Fe^{III} axial ligation	CO adducts				
		B-band	Q-bands		axial ligation[a]	ref
$HasA_{SM}$ pH 9.2	Tyr-Fe-His	413	534	568	O-Fe-CO	this work
$HasA_{SM}$ pH 7.5	Tyr-Fe-His	413	535	568	O-Fe-CO	this work
$HasA_{SM}$(H83A)	H_2O-Fe-His Fe-His	413	534	565	O-Fe-CO	*30*, this work
$HasA_{SM}$(H32A)	nyr[b]	413	534	567	O-Fe-CO	this work
*h*HO-1(H25Y)	Tyr-Fe	412	536	566	H_2O-Fe-CO	*53*
p22HBP	nr[c]	416	537	567	?-Fe-CO	*51*
BSA	nr[c]	419	538	567	?-Fe-CO	*51*
$HasA_{SM}$(Y75A)	nyr[b]	417	538	569	His-Fe-CO	this work
SW Mb(HisF8Tyr)	Tyr-Fe	418	536	568	His-Fe-CO	*19*
human Mb(H93Y)	Tyr-Fe	420	539	567	His-Fe-CO	*18*
Hb M Iwata	Tyr-Fe	420.2	539	569	His-Fe-CO	*28*
Hb M Boston	Tyr-Fe	420.8	539	569	His-Fe-CO	*28*
Hb M Hyde Park	Tyr-Fe	419.6	539	569	His-Fe-CO	*28*
Hb M Saskatoon	Tyr-Fe-His	418.8	539	569	His-Fe-CO	*28*
SW Mb(HisE7Tyr)	Tyr-Fe-His	424	542	574	His-Fe-CO	*19*
catalase	Tyr-Fe	427	545	580	Tyr-Fe-CO	*29*

[a] O indicates either OH_2 or Tyr ligand. [b] nyr: Not yet reported. [c] nr: Not reported.

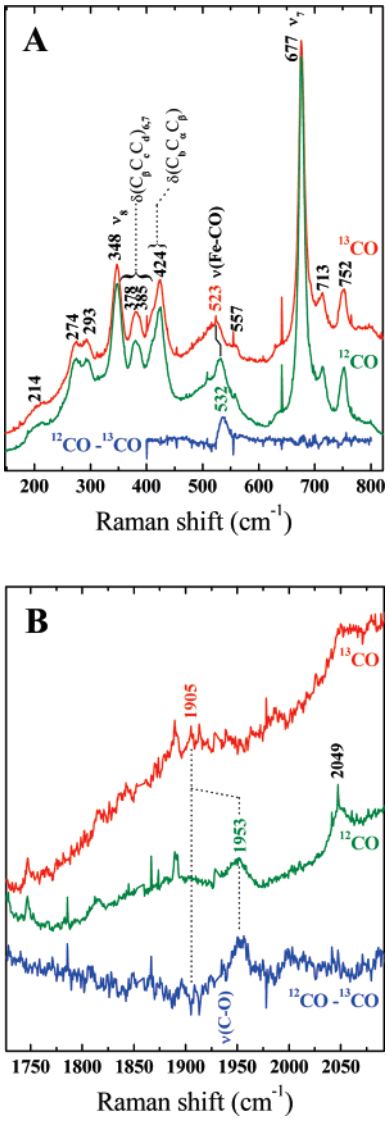

FIGURE 3: Isotope resonance Raman data for WT $HasA_{SM}$-CO. (A) Low-frequency region and (B) high-frequency region of the 413.1 nm excited resonance Raman spectrum of the isotopomers of $HasA_{SM}$-CO. The 80 μM WT protein in 100 mM Tris/HCl, pH 8.0 was reduced with sodium dithionite under an atmosphere of CO.

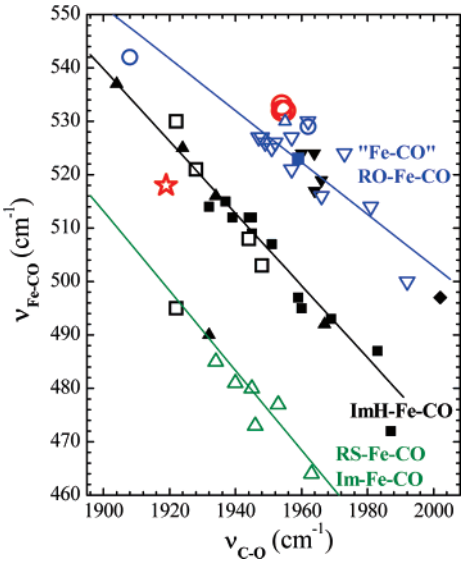

FIGURE 4: Correlation plots for Fe-CO and C-O stretching frequencies for heme proteins and model compounds. ν_{Fe-CO} versus ν_{C-O} for $HasA_{SM}$(Y75A), red ☆; WT $HasA_{SM}$, $HasA_{SM}$(H32A), $HasA_{SM}$(H83A), red ○; globins, ■; cytochrome *c* peroxidase, □; cytochrome P450s, green △; horseradish peroxidases, ▲; cytochrome oxidases, ▼; 5-coordinate model compounds, ▽; p22HBP, blue ■; FePPIX, blue △; C_2Cap(NMeIm), ◆; catalase and *h*HO-1(H25Y), blue ○. The green line correlates ν_{Fe-CO} with ν_{C-O} for 6c Fe-CO adducts in which the sixth ligand is a thiolate or an imidazolate; the black line represents Fe-CO adducts with histidine (neutral imidazole) as the sixth ligand; and the blue line represents a compilation of "5-coordinate" model complexes and heme proteins.

The spin state marker band, ν_3, occurs at 1499 cm^{-1} in rR spectra of WT $HasA_{SM}$-CO from pH 7.5 to 9.2 (Figure 5). The band at 1475 cm^{-1} is attributed to six-coordinate (6c), high-spin (HS) ferric heme (*30*) that was not converted to the ferrous CO adduct. This frequency lies at the low end of the ν_3 range for 6c HS ferric hemes and is consistent with a similarly low ν_3 frequency for the 5c HS heme catalases (*31*). On the basis of this small sampling, low ν_3 frequencies appear to be characteristic of HS hemes having proximal Tyr ligands. Attempts to observe ferrous WT $HasA_{SM}$ by rR via photolysis of the Fe-CO bond at high laser powers were

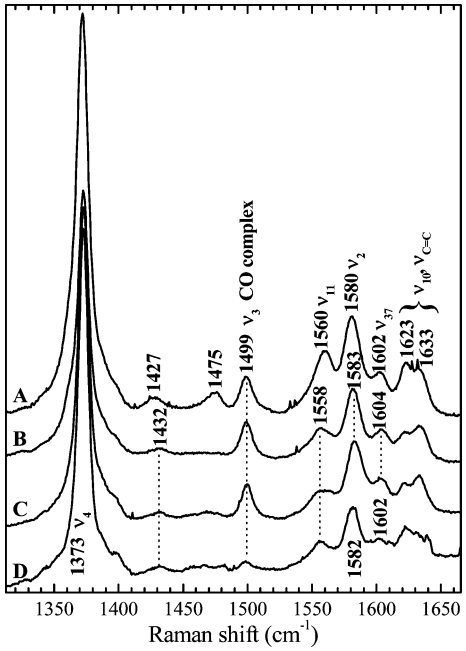

FIGURE 5: High-frequency resonance Raman spectra of (A) WT $HasA_{SM}$-CO, 100 mM Tris/HCl, pH 8.0; (B) $HasA_{SM}$(H83A)-CO; (C) $HasA_{SM}$(H32A)-CO; and (D) $HasA_{SM}$(Y75A)-CO. Spectra were obtained with 413.1 nm excitation and 3 mW laser power.

unsuccessful. The oxidation state marker ν_4 for ferrous $HasA_{SM}$ would be expected near 1355 cm^{-1}. The ν_4 band for WT $HasA_{SM}$-CO occurs at 1372 cm^{-1}. When $HasA_{SM}$-CO was subjected to 30 mW of laser illumination at 413.1 nm, no ν_4 intensity in the frequency range characteristic of ferrous $HasA_{SM}$ was detected. The inability to photodissociate WT $HasA_{SM}$-CO is consistent with the behavior recently predicted for 5c heme-COs or CO ligated to heme with a weak trans ligand (*32*).

$HasA_{SM}$(H32A)-CO. Although the reduction potential of −350 mV for $HasA_{SM}$(H32A) is much less negative than the −550 mV value for WT $HasA_{SM}$, the mutant protein is not readily reduced by sodium dithionite. The CO complex of ferrous $HasA_{SM}$(H32A) could only be formed upon treating a CO-saturated solution of the ferric protein with excess dithionite. Its UV−vis spectrum is comparable to that of WT $HasA_{SM}$-CO, supporting the hypothesis that the axial histidine (His32) is not a heme ligand in WT $HasA_{SM}$-CO (Figure 2 and Table 1). Resonance Raman spectra of $HasA_{SM}$-(H32A)-CO are also very similar to those observed for WT $HasA_{SM}$-CO. The natural abundance CO and ^{13}CO isotope data for $HasA_{SM}$(H32A)-CO are shown in Figure 6. The ν_{Fe-CO} band shifts from 532 to 526 cm^{-1}; the δ_{Fe-CO} band is also observed in this spectrum and shifts from 569 to 547 cm^{-1} in the ^{13}CO complex. The ν_{C-O} band shifts from 1955 to 1912 cm^{-1}. These frequencies place $HasA_{SM}$(H32A)-CO very close to the WT $HasA_{SM}$-CO complex on the ν_{Fe-CO}/ν_{C-O} correlation plot in Figure 4. This similarity is further evidence that His32 is not the proximal ligand in WT $HasA_{SM}$-CO.

The $HasA_{SM}$(H32A)-CO complex was examined at pH 7.2 and 10.0. Both the UV−vis and the high-frequency rR spectra indicate that the CO complex is insensitive to pH over this range. Even with high laser powers, neither 5c HS ferrous $HasA_{SM}$(H32A) nor ferric $HasA_{SM}$(H32A) accumulated to detectable levels, suggesting that either CO recombination is ultrafast or photodissoication of the heme-CO is not readily achieved.

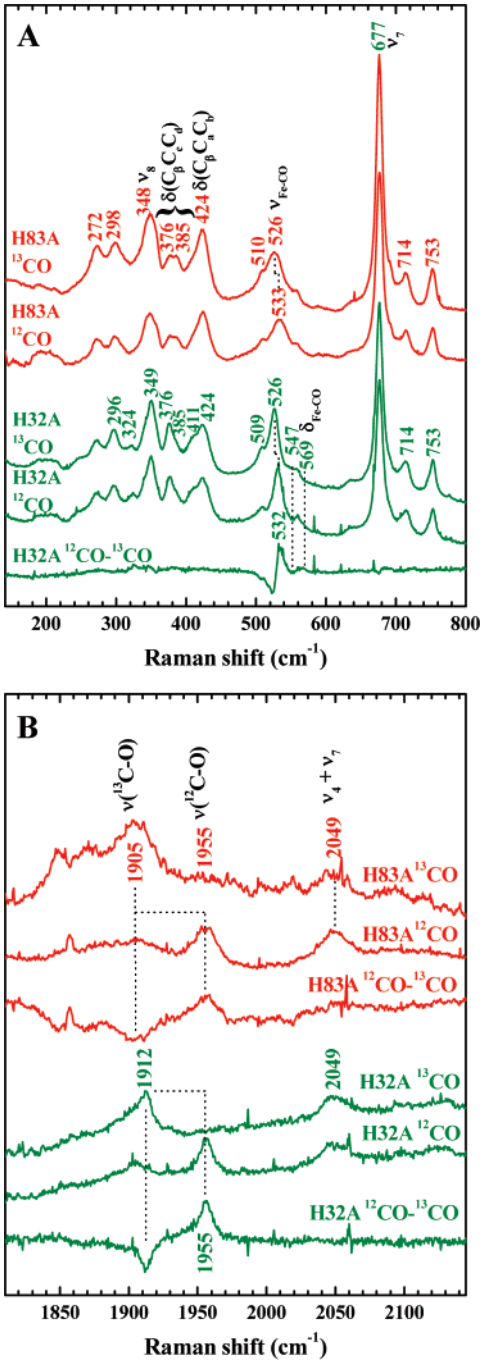

FIGURE 6: Resonance Raman spectra of $HasA_{SM}$(H83A)-CO (red) and $HasA_{SM}$(H32A)-CO (green). (A) Low-frequency region and (B) high-frequency regions of the 413.1 nm excited resonance Raman spectra. $HasA_{SM}$(H83A) and $HasA_{SM}$(H32A) concentrations were 45 and 54 μM, respectively. Both proteins were in 100 mM sodium phosphate buffer, pH 7.2 and were reduced with sodium dithionite under an atmosphere of CO.

$HasA_{SM}$(H83A)-CO. The reduction potential of $HasA_{SM}$-(H83A) is also very low at −400 mV. Consequently, the protein is not readily reduced by sodium dithionite, and ferrous $HasA_{SM}$(H83A)-CO could only be obtained by saturating the protein solution with CO prior to reduction. UV−vis spectra showing the formation of $HasA_{SM}$(H83A)-CO after the addition of excess dithionite are shown in the inset of Figure 2. The isosbestic behavior during this reaction (i.e., isosbestic points at 515 and 595 nm) indicate that

ferrous $HasA_{SM}$(H83A) does not build up to detectable levels during the reaction, consistent with the 5c, ferrous heme being trapped by CO as it forms. The ν_{Fe-CO} and ν_{C-O} frequencies for $HasA_{SM}$(H83A)-CO are similar to those observed for WT $HasA_{SM}$-CO and $HasA_{SM}$(H32A)-CO (Figure 6). We recently showed that ferric $HasA_{SM}$(H83A) has His32 as an axial ligand and that the sixth heme coordination site is vacant or occupied by a water ligand at neutral pH (*30*). Hence, if CO binds to the Tyr75 side of the heme in ferrous $HasA_{SM}$(H83A), a ν_{Fe-CO}/ν_{C-O} correlation consistent with imidazole or imidazolate ligation would be expected. This is not the case, as shown in Figure 4. The positions of CO complexes of WT and His mutants on the ν_{Fe-CO}/ν_{C-O} correlation line pose two possibilities. As these three complexes fall near the line that has been associated with 5c heme carbonyls, the coordination site trans to CO may be vacant. Alternatively, this position could be consistent with a weak axial ligand bond, such as that between iron and the phenolic oxygen atom of tyrosine or a water molecule.

Ferrous $HasA_{SM}$(Y75A). Mutation of the axial Tyr75 greatly facilitates reduction of the heme. The reduction potential of $HasA_{SM}$(Y75A) is the highest among this series of $HasA_{SM}$ proteins at −320 mV. Accordingly, reduction of the protein was achieved with a 10-fold excess of reducing equivalents from sodium dithionite. The B-band maximum shifts from 410 to 426 nm upon reduction (black and red spectra, respectively, in the inset of Figure 7A). After 30 min of laser irradiation during the course of acquiring a 441.6 nm excited rR spectrum, the B-band broadens, exhibiting a new feature at ∼434 nm with nearly the same absorbance as that at 426 nm (green spectrum, inset of Figure 7A). Both rR (vide infra) and UV−vis absorbance features show that this spectral signature does not evolve further with additional equilibration or laser irradiation time. Therefore, the change is unlikely to be the result of light-induced or thermal protein degradation, consistent with ferrous $HasA_{SM}$(Y75A) having reached equilibrium. The aforementioned absorbance features can be interpreted in two ways. First, the positions of the Soret features are consistent with a mixture of 6c (His-Fe-His, λ_{max} = 426 nm) and 5c (Fe-His, λ_{max} = 434 nm) ferrous hemes, respectively. The rR spectrum exhibits a ν_4 band, the oxidation state (or porphyrin π^*) marker, at 1354 cm^{-1}, a frequency typical of ferrous, pentacoordinate hemes. Two frequencies, 1466 and 1491 cm^{-1}, are observed in the region characteristic of the coordination state marker, ν_3. They are consistent with the presence of both 5c HS and 6c LS ferrous hemes, respectively (Figure 7A). Although, without rR cross-sections, relative rR intensities are generally unreliable indicators of corresponding populations, the large disparity between the intensities of the ν_3 bands in Figure 7A is inconsistent with the aforementioned similar B-band intensities. This inconsistency suggests an alternative interpretation of these data. There are examples of 5c HS ferrous hemes that exhibit split Soret bands. Although these are *c*-type cytochromes (*33*, *34*), their absorbance spectra are strikingly similar to the equilibrium spectrum in the inset of Figure 7A. Thus, it is possible that the split Soret band is a signature of the 5c HS ferrous $HasA_{SM}$(Y75A). This interpretation finds further support in the lack of high-frequency shoulders on the 5c HS ν_4 and ν_2 bands, where the corresponding LS bands of ferrous hemes having the bis-His axial ligand set tend to occur. Additionally, the low-frequency rR spectra exhibit a prominent band at 227 cm^{-1} (Figure 7B). In conjunction with this Raman shift, the increased relative intensity of this band in the spectrum excited at 441.6 nm (Figure 7B, spectrum b) over that of the 413.1 nm spectrum (Figure 7B, spectrum a) constitutes compelling evidence for assignment of the 227 cm^{-1} band to a mode having significant Fe-His stretching character in a 5c HS heme. Correlations have been established between ν_{Fe-His} frequency and φ, the dihedral angle between the proximal ImH plane and the closest trans-N_{pyrr}-Fe-N_{pyrr} axis/plane, for both neutral imidazole and imidazolate (*35*) While the 227 cm^{-1} frequency of ν_{Fe-His} is slightly

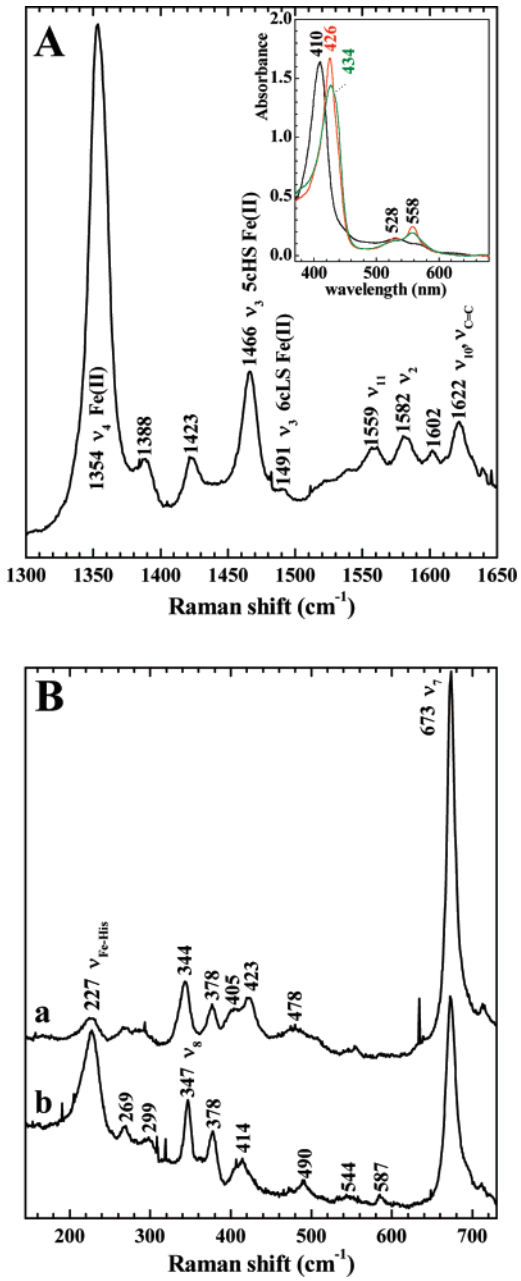

FIGURE 7: (A) High-frequency region of the Soret (413.1 nm) excited rR spectrum of ferrous $HasA_{SM}$(Y75A). Inset: UV−vis absorbance spectra of ferric (black), ferrous (green), and CO complex (red) of $HasA_{SM}$(Y75A). (B) Low-frequency rR spectrum of $HasA_{SM}$(Y75A) with (a) 413.1 nm excitation and (b) 441.6 nm excitation. $HasA_{SM}$(Y75A) was 100 μM in 100 mM Tris/HCl, pH 8.0. Laser power was 10 mW at the sample with both excitation frequencies.

higher than those observed for ferrous Hb and Mb (218−224 cm^{-1}) (*36*, *37*), it is considerably lower than those observed for peroxidases (i.e., ν_{Fe-Im-} occurs at 244 cm^{-1} for HRP (*38*)) and falls on the neutral ImH correlation line. These data constitute compelling evidence that the 5c ferrous $HasA_{SM}$(Y75A) retains axial histidine ligation. As His32 provides the axial ImH ligand in the crystal structure of ferric WT $HasA_{SM}$ (*20*), this residue is a reasonable candidate for the axial His in the 5c HS ferrous form of $HasA_{SM}$(Y75A). A second axial ligand must be available to coordinate in the initial 6c LS $HasA_{SM}$(Y75A) that forms upon reduction of the heme. In the ferric WT $HasA_{SM}$ structure, His83 is hydrogen bonded to the phenolate oxygen atom of Tyr75 (*20*). The distance between the $N_{\delta 1}$ of His83 and the iron atom is only 4.09 Å. The Y75A mutation reduces the steric bulk of the amino acid side chain between the heme iron and the His83, allowing His83 to adopt a non-native conformation and to become an axial ligand. Notably, the double mutant $HasA_{SM}$(H32A/Y75A) is still able to bind heme with a significant affinity (*22*), and it has been shown that in the gallium protoporphyrinIX/$HasA_{SM}$(Y75A) complex, His83 Nδ1 coordination to the heme iron is possible (*39*). Thus, we propose that the heme ligands in 6c LS ferrous $HasA_{SM}$(Y75A) are His32 and His83.

$HasA_{SM}$(Y75A)-CO. Ferrous $HasA_{SM}$(Y75A)-CO was generated by equilibrating the reduced protein solution under 1 atm of CO. The Fe-CO stretching band at 518 cm^{-1}, the Fe-C-O bend at 586 cm^{-1}, and the C-O stretch at 1919 cm^{-1} were identified by ^{13}CO substitution and are shown in Figure 8. The frequencies differ significantly from those of WT $HasA_{SM}$-CO, $HasA_{SM}$(H32A)-CO, and $HasA_{SM}$(H83A)-CO adducts. It is unique among these proteins in falling on the imidazole ν_{Fe-CO}/ν_{C-O} correlation line (Figure 4). Since both 5c and 6c ferrous forms of $HasA_{SM}$(Y75A) retain His32 as an axial ligand, it is likely that His32 is the proximal ligand in $HasA_{SM}$(Y75A)-CO. The position of a point on a given correlation line reflects the degree of π back-bonding in the Fe-CO moiety, which is governed by both Fe-C-O geometry and the distal electrostatic landscape (*25*, *40*). Off-axis Fe-C-O distortion and a negative charge weaken back-bonding that, without other factors such as hydrogen bonding, is characterized by positions to the right (low) on the correlation line. Interactions of the CO ligand with positively charged or H-bond donating residues on the distal side of the heme are known to enhance π back-bonding, thereby positioning points high on the imidazole line (i.e., $\nu_{Fe-CO} \gtrsim 520$ cm^{-1} and $\nu_{C-O} \lesssim 1935$ cm^{-1}) (*41*). $HasA_{SM}$(Y75A)-CO data fall in the range consistent with a distal interaction between a H-bond donor and the terminal O atom of CO. As His83, which normally hydrogen bonds with Tyr75 in WT $HasA_{SM}$ (*20*), is present in $HasA_{SM}$(Y75A), it is a likely candidate for the H-bond donor in $HasA_{SM}$(Y75A)-CO. Participation of water in a H-bonding network cannot be discounted.

$I(\nu_4)/I(\nu_3)$ as an Indicator of the Trans Ligand Field. The high-frequency rR spectrum of $HasA_{SM}$(Y75A)-CO is similar to that of other His-Fe-CO hemes (*28*), consistent with its proximal ligand being different from that of the WT protein and of the two His mutants. High-frequency rR spectra of WT $HasA_{SM}$-CO, $HasA_{SM}$(H32A)-CO, $HasA_{SM}$(H83A)-CO, and $HasA_{SM}$(Y75A)-CO are compared in Figure 5. While the ν_4 band for all four proteins occurs near 1373 cm^{-1}, consistent with the formation of ferrous heme carbonyl

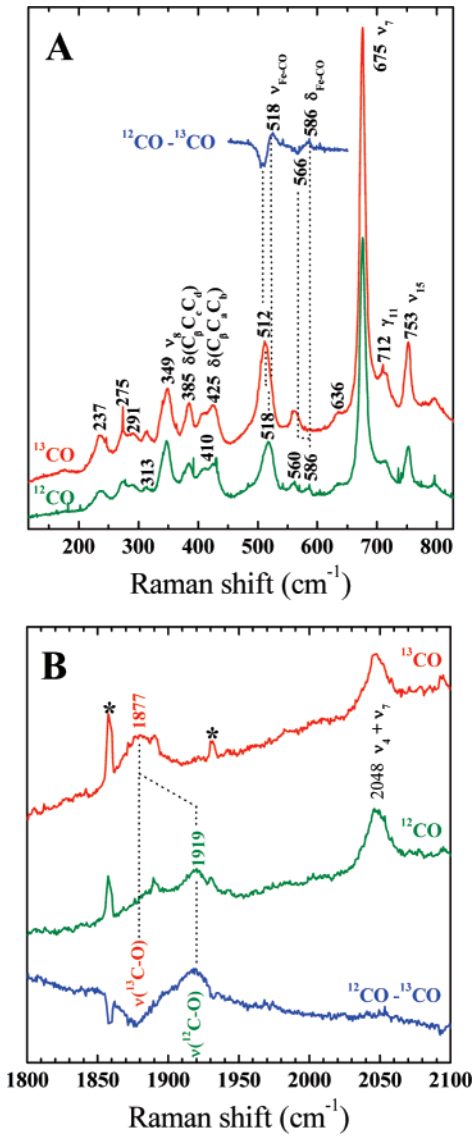

FIGURE 8: Soret excited (413.1 nm) resonance Raman spectra of $HasA_{SM}$(Y75A)-CO isotopologues. (A) Low-frequency and (B) high-frequency regions of the spectra. The 100 μM reduced protein samples from Figure 7 were placed under an atmosphere of CO. The asterisk marks a plasma emission line from the Kr^+ laser.

complexes, it is interesting to note that the relative intensities of ν_4 and ν_3 differ between $HasA_{SM}$(Y75A)-CO ($I(\nu_4)/I(\nu_3)$ = 23:1) and the other $HasA_{SM}$ proteins (WT $HasA_{SM}$-CO, $I(\nu_4)/I(\nu_3)$ = 11:1; $HasA_{SM}$(H83A)-CO, $I(\nu_4)/I(\nu_3)$ = 8:1; and $HasA_{SM}$(H32A)-CO, $I(\nu_4)/I(\nu_3)$ = 7:1). In the case of $HasA_{SM}$(Y75A)-CO, which contains a proximal His ligand (vide supra), the $I(\nu_4)/I(\nu_3)$ ratio is 2−3 times greater than in the other three constructs. Large $I(\nu_4)/I(\nu_3)$ ratios are typical of His-Fe-CO protein complexes such as Hb-CO (*42*), Mb-CO (*43*), HO-CO (*43*), sGC-CO (*44*), and HemAT-B-CO (*45*). Proteins with the His/Tyr axial ligand set in the ferric form and His-Fe-CO ligation in their ferrous CO complexes, such as Saskatoon HbM (*28*) and CcmE (~16:1) (*12*), also have large $I(\nu_4)/I(\nu_3)$ ratios. The $I(\nu_4)/I(\nu_3)$ ratio for the heme catalase-CO complex, which contains a Tyr-Fe-CO moiety, is only ~4.4:1 (*29*). Thus, the small $I(\nu_4)/I(\nu_3)$ ratios that characterize the rR spectra of the WT, (H32A), and (H83A) $HasA_{SM}$-CO complexes are characteristic of either a weak or absent proximal bond (*29*).

Roles of Hydrogen Bonding in the Stability of HasA_{SM}. Along with the two Fe-L_{axial} bonds, $HasA_{SM}$ is stabilized by hydrogen bonding within the heme pocket, including interactions between the heme periphery and the protein. In addition to the aforementioned hydrogen bond between the side chains of Tyr75 and His83, Figure 1 reveals that the phenol side chain of Tyr137 serves as a H-bond donor to the backbone carbonyl of heme ligand, His32, whose coordinated ImH is a H-bond donor to the backbone carbonyl of Asn41. The backbone amide groups of Gly35 and Asn34 serve as H-bond donors to the carboxylate groups of the heme propionates. It has been reported that decreased H-bond donation to the propionate groups of Mb elicits diminution of the propionate bending frequency (*46*). Accordingly, changes in the H-bonding environments of the heme propionate groups are expected to affect the frequencies of the propionate bending modes ($\delta(C_\beta C_c C_d)$) in $HasA_{SM}$ and its mutants. In the spectral region where the propionate bending modes are expected, WT $HasA_{SM}$-CO has bands at 378 and 385 cm^{-1}. The frequencies of these two bands indicate that there are two H-bonding environments available to the propionate groups, one with a weaker H-bonding interaction (378 cm^{-1}) and one with a stronger H-bonding network (385 cm^{-1}). When the coordinating Tyr75 is removed, the stronger H-bonding environment is favored, as a prominent $\delta(C_\beta C_c C_d)$ band at 385 cm^{-1} is observed for $HasA_{SM}$(Y75A)-CO (Figure 8A). Because CO binds on the Tyr75 side of the heme in this mutant (vide supra), the heme is not displaced away from the Asn34 and Gly35 residues but probably pulled toward these H-bonding residues by the Fe-His32 bond. Consequently, H-bonding interactions between Asn34 and Gly35 and the heme propionates are strengthened as reflected by the increase in intensity of the higher frequency $\delta(C_\beta C_c C_d)$ band.

The opposite occurs when His32 is removed from the heme binding site. For $HasA_{SM}$(H32A)-CO, the band at 376 cm^{-1} becomes the dominant $\delta(C_\beta C_c C_d)$ band, and the 385 cm^{-1} band decreases in intensity, becoming a shoulder on the 376 cm^{-1} band (Figure 6A). The intensity increase at 376 cm^{-1} and the concomitant decrease at 385 cm^{-1} are consistent with an overall loss in H-bond strength involving the heme propionate groups. As both Asn34 and Gly35 are on the His32 side of the heme, this weaker H-bonding environment is consistent with the heme being pulled toward Tyr75 when position 32 is occupied by a non-coordinating amino acid. An alternate explanation is that the loop containing Asn34 and Gly35 has greater conformational freedom in the H32A mutant than in WT. This loop mobility alone or in concert with an Fe-Tyr75 interaction that is either direct or modulated by water could be responsible for a weaker H-bonding environment in $HasA_{SM}$(H32A)-CO.

Disruption of the axial ligands in the heme binding pocket appears to have a greater effect on the H-bonding environment than alteration of the His83-Tyr75 H-bonding interaction. Two propionate bending bands of roughly equal intensity are observed at 376 and 385 cm^{-1} for $HasA_{SM}$-(H83A)-CO, indicating that its H-bonding environment is similar to that in WT $HasA_{SM}$-CO.

The results presented herein show that the His32 side chain is uniquely and preferentially displaced upon binding of CO to the ferrous heme. A trans His ligand is only seen when Tyr75 is missing from the heme pocket. Furthermore, frequencies of the peripheral propionate modes in the heme-CO complexes that contain Tyr75 report that the H-bonding interaction with the propionate groups is weakened, suggesting that Tyr75 continues to interact with the heme iron in the CO complexes.

DISCUSSION

Displacement of His32 by CO in Ferrous WT HasA_{SM}. The hemes in the mutated subunits of ferric HbM Iwate, HbM Hyde Park, HbM Saskatoon, and HbM Boston have axial phenolate ligands from Tyr^- at position F8 or E7 (*14*). Upon reduction, however, these phenolate ligands are replaced by the imidazole side chain of histidine, as demonstrated by ν_{Fe-His} bands near 215 cm^{-1} in their rR spectra (*28*). Characterization of these HbM-CO complexes revealed that they are 6c complexes that fall on the histidine ν_{Fe-CO}/ν_{C-O} correlation line. Since WT $HasA_{SM}$ has the His/Tyr axial ligand set in its ferric form, it is tempting to predict that Tyr75 would be preferentially lost in the reduced form. In contrast to this prediction, WT $HasA_{SM}$-CO, $HasA_{SM}$-(H32A)-CO, and $HasA_{SM}$(H83A)-CO are all located above the histidine line on the ν_{Fe-CO}/ν_{C-O} correlation plot in Figure 4. This constitutes compelling evidence that these three CO complexes have weak proximal ligand fields, which is inconsistent with a proximal His ligand. A number of situations have been shown to result in CO complexes located above the histidine correlation line, and they suggest several interpretations of the $HasA_{SM}$-CO position.

6c Complex in Which the Fe-C Bond Is Compressed as a Result of a Steric Interaction on the His32 Side of the Heme. Compression of the Fe-CO bond can result from a variety of steric interactions between the CO ligand and its immediate protein environment. Such Fe-CO bond compression has been reported for cytochrome aa_3-type terminal oxidases having dinuclear heme-copper catalytic sites (*47*−*50*). In these oxidases, the distal steric constraint of the CO ligand is attributed to a strong interaction between the copper atom and the heme-bound CO. The oxidases and a model complex of their active site (C_2Cap(NMeIm) (*25*)) lie well above the histidine line of the ν_{Fe-CO}/ν_{C-O} correlation plot and in the region of what has been called the 5c line (Figure 4 (▼ and ◆) and Table 2). However, despite their positions on the correlation plot, there is compelling evidence that the CO adducts of C_2Cap(NMeIm) and these terminal oxidases have imidazole ligands from proximal His residues. As shown in the crystal structure of ferric $HasA_{SM}$, there are two tyrosines, Tyr55 and Tyr137, on the His32 side of the heme. However, the edge of the phenolate ring closest to the iron atom lies at least 6 Å from it (Tyr137, 6.1 Å and Tyr55, 7.9 Å) (*20*). An interaction between one of these Tyr side chains and bound CO, analogous to that observed in the C_2Cap(NMeIm) model complex, would require that one of the tyrosines move significantly to position its phenolate ring above the Fe-CO moiety. As these residues reside on a helix and a β sheet, this would require substantial conformational reorganization. Moreover, it is likely that the conformational flexibility of the heme binding loops would serve to relax any steric interaction strong enough to compress the Fe-CO bond.

5c CO Complexes with No Axial Heme Ligands from the Protein. Carbonyl complexes of numerous model compounds have been reported to be 5c with their ν_{Fe-CO} and ν_{C-O}

Table 2: Raman Frequencies for Comparison of $HasA_{SM}$-CO Adducts with Heme-CO Complexes Having Weak, Compressed, or Missing Proximal Bonds[a]

CO complexes	ν_{Fe-CO}	ν_{C-O}	ν_2	ν_3	ν_4	ref
WT $HasA_{SM}$	532 (523)	1954 (1905)	1580	1499	1372	this work
$HasA_{SM}$(H32A)	532 (526)	1955 (1912)	1583	1499	1373	this work
$HasA_{SM}$(H83A)	533 (526)	1955 (1905)	1583	1499	1373	this work
$HasA_{SM}$(Y75A)	518 (512)	1919 (1877)	1582	1499	1373	this work
6c CO adducts with weak proximal bonds						
human Mb(H93Y)	497, 528	nr[b]	1586	1502	1373	*18*
catalase(C-100)	542 (539)	1908 (1863)	1588	1501	1376	*29*
human HO-1(H25Y)	529 (524)	1962 (1917)	nr	nr	nr	*53*
p22HBP	523	1959	1583	1499	1372	*51*
[Fe(PPIX)] (80% glycerol)	530 (525)	1955	nr	nr	nr	*54*
6c CO adducts with steric factors that cause distal compression of Fe-CO						
R. sphaeroides α aa_3-type cytoxidase	519 (506)[c]	1966 (1876)[c]	nr	nr	nr	*47, 48*
bovine α cyt aa_3	520	1964	nr	nr	nr	*49*
E. coli cyt bo_3	524	1960	nr	nr	nr	*50*
C_2Cap (NMeIm)	497 (493)	2002 (1958)	nr	nr	nr	*25*

[a] All frequencies in cm^{-1}. Values in parentheses are frequencies of the ^{13}CO isotopologues. [b] nr: not reported. [c] Data for the $^{13}C^{18}O$ adduct.

frequencies, placing them on a 5c correlation line above the histidine line (*24*) (see Table 2 and Figure 4). The CO adduct of the heme/BSA complex, which is stabilized by hydrophobic interactions without specific heme ligands, also falls on this 5c correlation line (*51*). Interestingly, the crystal structure of the analogous heme/human serum albumin complex reveals a Tyr ligand coordinated to the ferric heme (*52*). Although the result has not been reported to date, based on the evidence presented herein, one would predict that the CO complex of heme/human serum albumin would fall on the 5c correlation line of the back-bonding correlation plot. The CO complexes of WT $HasA_{SM}$, $HasA_{SM}$(H32A), and $HasA_{SM}$(H83A) fall near one another and in the vicinity of the 5c correlation line. Accordingly, it is reasonable to hypothesize that all three of these HasA proteins form pentacoordinate CO adducts in which axial ligation between the heme and the protein has been lost. However, it is not clear as to whether that position on the correlation plot can differentiate between 5c CO complexes and 6c CO complexes having a weak proximal Fe-L bond (*23*). As an example of this ambiguity, Tyr ligation of the heme in *h*HO-1(H25Y) is lost upon reduction with sodium dithionite. The FeCO vibrational frequencies for its CO complex place it well above the line correlating ν_{Fe-CO} and ν_{C-O} for trans His ligation and among the 5c heme carbonyls. Thus, *h*HO-1(H25Y)-CO has been proposed to be either a 5c complex or 6c complex with a weak sixth ligand, such as a water molecule (*53*).

6c CO Complexes with a Weak Fe-L_{axial} Bond Trans to the CO Ligand. Given that (a) the Fe-CO vibrational signatures are nearly identical for WT $HasA_{SM}$, $HasA_{SM}$-(H32A), and $HasA_{SM}$(H83A) and (b) their (ν_{Fe-CO}/ν_{C-O}) points fall above the imidazole and imidazolate correlation lines, it seems reasonable to suggest that CO binds on same side of the heme in these cases and that it displaces the His32 heme ligand. In the $HasA_{SM}$(H32A) case, the axial histidine has already been removed by mutation. On the basis of the crystal structure of ferric WT $HasA_{SM}$ (*20*), the closest potential ligands on the His32 side of the heme are Tyr55 and Tyr137. However, their phenol oxygen atoms are more than 7 Å from the iron atom (the phenol oxygen-iron distances are 7.1 and 7.2 Å, respectively, in the 1B2V structure). While the possibility of one of these Tyr oxygen atoms moving to within coordination distance of the iron in $HasA_{SM}$(H32A)-CO cannot be discounted, this seems an unlikely price to pay for the formation of a weak Fe^{II}-O(H)-Ph bond. Thus, CO is concluded to bind to $HasA_{SM}$(H32A) in the coordination site that is vacated by the H32A mutation. His83 is known to stabilize the ferric holo$HasA_{SM}$ complex by accepting a hydrogen bond from the heme-bound phenol OH group of Tyr75 (*20*, *21*). Since the mutation of His83 decreases the protein affinity for heme (*21*), it is reasonable to predict that this mutation destabilizes the Fe-Tyr75 bond. In fact, in ferric $HasA_{SM}$(H83A), the Fe-His32 bond is maintained, while the Fe-Tyr75 bond is broken (*30*). However, if CO bound to the ferrous form of $HasA_{SM}$(H83A) on the Tyr75 side of the heme, His32 would be its trans ligand, and $HasA_{SM}$(H83A)-CO should fall on the imidazole correlation line. It does not. As such, CO binding appears to occur with the displacement of the His32 ligand in WT $HasA_{SM}$ and in $HasA_{SM}$(H83A), placing it on the His32 side of the heme. The Fe-L_{axial} bond in WT $HasA_{SM}$-CO, $HasA_{SM}$-(H83A)-CO, and $HasA_{SM}$(H32A)-CO is weak based on the similarity of their ν_{Fe-CO}/ν_{CO} positions on the correlation plot to those of [Fe(PPIX)CO] (*54*) and *h*HO-1(H25Y) (*53*) (Figure 4: blue △, Fe(PPIX) and blue ○, *h*HO-1(H25Y)). It has been proposed that these two CO complexes have weak Fe-O bonds due to a coordinated water molecule trans to CO (*53*, *54*). Recent computational results corroborate this hypothesis and suggest that the correlation line commonly referred to as the 5c line characterizes 6c carbonyl complexes with oxygen donor ligands trans to CO (Linder, D. P., and Rodgers, K. R., unpublished results).

In the case of $HasA_{SM}$-CO, except for the Tyr75 ligand and its H-bond partner His83, that side of the heme pocket is rather hydrophobic. Therefore, in the three $HasA_{SM}$ constructs containing Tyr75, the Tyr75 side chain is a likely trans ligand, analogous to that in catalase-CO. At this time, however, the possibility of a trans water molecule in one or more of these $HasA_{SM}$-COs cannot be discounted. The FeCO Raman frequencies of the $HasA_{SM}$-COs differ from those of catalase-CO. If one generates a ν_{Fe-CO}/ν_{C-O} line using only data points thought to be O-Fe-CO complexes (catalase-CO, [Fe(PPIX)CO], HO-1(H25Y)-CO, $HasA_{SM}$-CO, $HasA_{SM}$-(H32A)-CO, and $HasA_{SM}$(H83A)-CO), catalase is the left-most point on the line. Positions to the left indicate Fe-C

and C-O bonds that are stronger and weaker, respectively, and correspond to stronger FeCO π back-bonding. If the position along this O-Fe-CO line is governed by the same distal factors as the position on the imidazole line, then points toward the left would be characteristic of electrostatic interaction with positive charge or H-bond donation to the bound CO. Both of these interactions are known to enhance π back-bonding. It is, therefore, proposed that the distal pocket of human erythrocyte catalase harbors a H-bond donor, possibly His75, as seen in the ferric cyanide complex (*55*, *56*). The FeCO Raman frequencies indicate that distal H-bonding is weak or absent in the $HasA_{SM}$-CO proteins reported here. Thus, the native His32 ligand is probably not involved in hydrogen bonding to the CO ligand of WT $HasA_{SM}$, as WT $HasA_{SM}$ and $HasA_{SM}$(H32A) CO adducts fall at very similar positions on the correlation line.

Why Does CO Displace His32 in Preference to Tyr75? Absent other factors, one would expect the relatively soft Fe(II) center to prefer coordination by proximal N_{His} over a harder O-bound ligand such as water or the phenol side chain of Tyr. The fact that the carbonyl complex is not coordinated by His32 suggests that other mitigating factors determine the first coordination sphere of the $HasA_{SM}$-CO complex. The aforementioned lack of H-bonding between the displaced ImH side chain of His32 and the CO ligand may hold the key to understanding this situation. Upon scission of the Fe-His32 bond, a modest conformational rearrangement would put the Tyr55 and Tyr137 side chains within reach of the imidazole side chain of His32. Intriguingly, Met140 is located between the side chains of Tyr55 and Tyr137, apparently keeping them available for H-bonding interactions by preventing H-bonding between them. The structural proximity of these residues is revealed in the crystal structure of the ferric state, which shows that the backbone carbonyl oxygen atom of His32 and the phenolic oxygen atom of Tyr 137 are within H-bonding distance (*20*). Hence, upon displacement of His32 by CO, the H-bonding interactions necessary to stabilize a His32-off state are readily available, leaving the bound CO ligand flanked by the hydrophobic side chains of Val37 and Met140. Analogously, non-bonded stabilization of a His-off state has been reported for the proximal imidazole in the pentacoordinate, proximal cyt *c*′-NO complex (*57*). Stabilization of a proximal His-off state in cyt *c*′ has been shown to facilitate intramolecular and perhaps physiologically relevant ligand exchange dynamics (*58*). This is possible because the *c*-type heme is covalently bound to the protein and cannot be released from it, even when the heme has no endogenous axial ligand(s). In contrast, the *b*-type heme of $HasA_{SM}$ is not covalently bound to the protein. Therefore, loss of an axial ligand is necessarily among the mechanistic steps that culminate in the release of heme from the protein. As the affinity of HasA(H32A) for ferric heme is close to that of the WT protein, mere dissociation of His32 is unlikely to drive release of heme from holo$HasA_{SM}$. However, non-bonded interaction(s) of the dissociated His32 may stabilize an intermediate conformer having a diminished affinity for heme. It was previously shown that the strength of the Fe-Tyr75 bond is modulated by the His83-Tyr75 H-bond (*59*). It has further been suggested that weakening of this H-band is a prelude to Fe-Tyr75 bond scission upon binding of $HasA_{SM}$ to $HasR_{SM}$ (*30*, *60*) (Wolff, N., Wandersman, C., and Lecroisey, A., unpublished results). To date, however, there is no definitive mechanistic evidence as to which bond, Fe-Tyr75 or Fe-His32, forms first in heme binding or breaks first in the heme release. Nevertheless, the results presented herein support the hypothesis that a His32-off state, such as that described above, is accessible. Thus, the stabilization of such a state by intramolecular H-bonding with Tyr135 and/or Tyr137 could be relevant to the uptake of ferric heme by apo-$HasA_{SM}$ and/or its release from holo-$HasA_{SM}$. In the complex reported here, formation of the His32-off state is clearly driven by the formation of the ferrous heme-CO complex. Its formation during uptake and/or release of ferric heme would have to be driven by other factors. As previously suggested (*59*), the formation of such states having an intermediate stability could be driven by $HasA_{SM}$-$HasR_{SM}$ interactions (*60*). Of potential importance, a pentacoordinate Tyr-liganded heme intermediate would maintain a relatively negative reduction potential, thereby precluding Fenton-type chemistry that might occur due to the reaction of ferrous heme with O_2. The proposed His32-off state of $HasA_{SM}$-CO is shown in Scheme 1.

Scheme 1

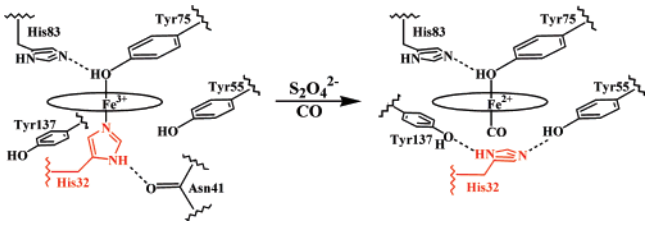

CONCLUSION

Proteins containing hemes that exhibit axial Tyr or His/Tyr coordination in the ferric state usually lose the tyrosine ligation in favor of a histidine ligation upon reduction. As a result, their CO complexes typically have His-Fe-CO axial ligation. It has been suggested that a tyrosine is the distal ligand in the alkaline ferrous form of *Clamidomonas* chloroplast hemoglobin, giving it Tyr-Fe-His axial heme coordination (*61*). Ferrous cytochrome *c* maturation protein, CcmE (*12*), was shown to have a histidine and most likely a tyrosine as axial ligands. However, in both cases, the CO complexes exhibit His-Fe-CO ligation. With the exception of catalase-CO (*29*), no hemoprotein CO complexes have been reported to have a proximal Tyr-derived phenol ligand. This work presents new examples of heme carbonyls possibly having Tyr-Fe-CO ligation. Additionally, loss of the axial histidine ligand upon CO binding in hemoproteins having the His/Tyr axial ligand set is described here for the first time. Most importantly, regardless of whether these $HasA_{SM}$-CO complexes are 5c or 6c, a lack of H-bonding between the displaced His32 and the CO ligands suggests that the ImH side chain of His32 is stabilized by other non-bonding interactions within the heme pocket. In accord with this behavior, it is herein proposed that an analogous His32 dissociated state occurs during the uptake and/or release of ferric heme.

ACKNOWLEDGMENT

The authors are grateful to Dr. P. Bianco for carrying out the voltammetry experiments and to Prof. C. Wandersman,

Dr. M. Delepierre, Dr. Douglas Linder, and Darci Block for their helpful discussions.

REFERENCES

1. Létoffé, S., Ghigo, J. M., and Wandersman, C. (1994) Iron acquisition from heme and hemoglobin by a *Serratia marcescens* extracellular protein, *Proc. Natl. Acad. Sci. U.S.A. 91*, 9876−9880.
2. Binet, R., and Wandersman, C. (1995) Protein secretion by hybrid bacterial ABC-transporters: Specific functions of the membrane ATPase and the membrane fusion protein, *EMBO J. 14*, 2298−2306.
3. Ghigo, J. M., Letoffe, S., and Wandersman, C. (1997) A new type of hemophore-dependent heme acquisition system of *Serratia marcescens* reconstituted in *Escherichia coli*, *J. Bacteriol. 179*, 3572−3579.
4. Binet, R., and Wandersman, C. (1996) Cloning of the *Serratia marcescens* hasF gene encoding the Has ABC exporter outer membrane component: A TolC analogue, *Mol. Microbiol. 22*, 265−273.
5. Létoffé, S., Redeker, V., and Wandersman, C. (1998) Isolation and characterization of an extracellular heme-binding protein from *Pseudomonas aeruginosa* that shares function and sequence similarities with the *Serratia marcescens* HasA hemophore, *Mol. Microbiol. 28*, 1223−1234.
6. Ochsner, U. A., Johnson, Z., and Vasil, M. L. (2000) Genetics and regulation of two distinct haem-uptake systems, phu and has, in *Pseudomonas aeruginosa*, *Microbiology (Reading, U.K.) 146*, 185−198.
7. Rossi, M. S., Fetherston, J. D., Letoffe, S., Carniel, E., Perry, R. D., and Ghigo, J. M. (2001) Identification and characterization of the hemophore-dependent heme acquisition system of *Yersinia pestis*, *Infect. Immun. 69*, 6707−6717.
8. Idei, A., Kawai, E., Akatsuka, H., and Omori, K. (1999) Cloning and characterization of the *Pseudomonas fluorescens* ATP-binding cassette exporter, HasDEF, for the heme acquisition protein HasA, *J. Bacteriol. 181*, 7545−7551.
9. www.sanger.ac.uk/Projects/E_carotovora, 2006.
10. Izadi, N., Henry, Y., Haladjian, J., Goldberg, M. E., Wandersman, C., Delepierre, M., and Lecroisey, A. (1997) Purification and characterization of an extracellular heme-binding protein, HasA, involved in heme iron acquisition, *Biochemistry 36*, 7050−7057.
11. Czjzek, M., Letoffe, S., Wandersman, C., Delepierre, M., Lecroisey, A., and Izadi-Pruneyre, N. (2007) The crystal structure of the secreted dimeric form of the hemophore HasA reveals a domain swapping with an exchanged heme ligand, *J. Mol. Biol. 365*, 1176−1186.
12. Uchida, T., Stevens, J. M., Daltrop, O., Harvat, E. M., Hong, L., Ferguson, S. J., and Kitagawa, T. (2004) The interaction of covalently bound heme with the cytochrome *c* maturation protein CcmE, *J. Biol. Chem. 279*, 51981−51988.
13. Williams, P. A., Fulop, V., Garman, E. F., Saunders, N. F., Ferguson, S. J., and Hajdu, J. (1997) Haem-ligand switching during catalysis in crystals of a nitrogen-cycle enzyme, *Nature (London, U.K.) 389*, 406−412.
14. Nagai, M., Yoneyama, Y., and Kitagawa, T. (1989) Characteristics in tyrosine coordinations of four hemoglobins M probed by resonance Raman spectroscopy, *Biochemistry 28*, 2418−2422.
15. Lecomte, J. T., Smit, J. D., Winterhalter, K. H., and La Mar, G. N. (1989) Structural and electronic properties of the liver fluke heme cavity by nuclear magnetic resonance and optical spectroscopy. Evidence for a distal tyrosine residue in a normally functioning hemoglobin, *J. Mol. Biol. 209*, 235−247.
16. Kraus, D. W., Wittenberg, J. B., Lu, J. F., and Peisach, J. (1990) Hemoglobins of the *Lucina pectinata*/bacteria symbiosis. II. An electron paramagnetic resonance and optical spectral study of the ferric proteins, *J. Biol. Chem. 265*, 16054−16059.
17. Das, T. K., Couture, M., Lee, H. C., Peisach, J., Rousseau, D. L., Wittenberg, B. A., Wittenberg, J. B., and Guertin, M. (1999) Identification of the ligands to the ferric heme of *Chlamydomonas* chloroplast hemoglobin: Evidence for ligation of tyrosine-63 (B10) to the heme, *Biochemistry 38*, 15360−15368.
18. Adachi, S., Nagano, S., Ishimori, K., Watanabe, Y., Morishima, I., Egawa, T., Kitagawa, T., and Makino, R. (1993) Roles of proximal ligand in heme proteins: Replacement of proximal histidine of human myoglobin with cysteine and tyrosine by site-directed mutagenesis as models for P-450, chloroperoxidase, and catalase, *Biochemistry 32*, 241−252.
19. Egeberg, K. D., Springer, B. A., Martinis, S. A., Sligar, S. G., Morikis, D., and Champion, P. M. (1990) Alteration of sperm whale myoglobin heme axial ligation by site-directed mutagenesis, *Biochemistry 29*, 9783−9791.
20. Arnoux, P., Haser, R., Izadi, N., Lecroisey, A., Delepierre, M., Wandersman, C., and Czjzek, M. (1999) The crystal structure of HasA, a hemophore secreted by *Serratia marcescens*, *Nat. Struct. Biol. 6*, 516−520.
21. Deniau, C., Gilli, R., Izadi-Pruneyre, N., Letoffe, S., Delepierre, M., Wandersman, C., Briand, C., and Lecroisey, A. (2003) Thermodynamics of heme binding to the $HasA_{SM}$ hemophore: Effect of mutations at three key residues for heme uptake, *Biochemistry 42*, 10627−10633.
22. Létoffé, S., Deniau, C., Wolff, N., Dassa, E., Delepelaire, P., Lecroisey, A., and Wandersman, C. (2001) Haemophore-mediated bacterial haem transport: Evidence for a common or overlapping site for haem-free and haem-loaded haemophore on its specific outer membrane receptor, *Mol. Microbiol. 41*, 439−450.
23. Spiro, T. G., and Wasbotten, I. H. (2005) CO as a vibrational probe of heme protein active sites, *J. Inorg. Biochem. 99*, 34−44.
24. Vogel, K. M., Kozlowski, P. M., Zgierski, M. Z., and Spiro, T. G. (2000) Role of the axial ligand in heme-CO backbonding; DFT analysis of vibrational data, *Inorg. Chim. Acta 297*, 11−17.
25. Ray, G. B., Li, X. Y., Ibers, J. A., Sessler, J. L., and Spiro, T. G. (1994) How far can proteins bend the FeCO unit? Distal polar and steric effects in heme proteins and models, *J. Am. Chem. Soc. 116*, 162−176.
26. Haladjian, J., Thierry-Chef, I., and Bianco, P. (1996) *Talanta 43*, 1125−1130.
27. Jin, Y., Nagai, M., Nagai, Y., Nagatomo, S., and Kitagawa, T. (2004) Heme structures of five variants of hemoglobin M probed by resonance Raman spectroscopy, *Biochemistry 43*, 8517−8527.
28. Nagai, M., Yoneyama, Y., and Kitagawa, T. (1991) Unusual carbon monoxide bonding geometry in abnormal subunits of hemoglobin M Boston and hemoglobin M Saskatoon, *Biochemistry 30*, 6495−6503.
29. Hu, S., and Kincaid, J. R. (1992) Resonance Raman studies of the carbonmonoxy form of catalase. Evidence for and effects of phenolate ligation, *FEBS Lett. 314*, 293−296.
30. Caillet-Saguy, C., Turano, P., Lukat-Rodgers, G. S., Czjzek, M., Guigliarelli, B., Izadi-Pruneyre, N., Rodgers, K. R., Delepelaire, P., and Lecroisey, A. (2007) Deciphering the structural role of Histidine 83 for heme binding in hemophore HasA, *J. Biol. Chem.*, submitted.
31. Sharma, K. D., Andersson, L. A., Loehr, T. M., Terner, J., and Goff, H. M. (1989) Comparative spectral analysis of mammalian, fungal, and bacterial catalases. Resonance Raman evidence for iron-tyrosinate coordination, *J. Biol. Chem. 264*, 12772−12779.
32. Ohta, T., Pal, B., and Kitagawa, T. (2005) Excited state property of hardly photodissociable Heme-CO adduct studied by time-dependent density functional theory, *J. Phys. Chem. B 109*, 21110−21117.
33. Andrew, C. R., Green, E. L., Lawson, D. M., and Eady, R. R. (2001) Resonance Raman studies of cytochrome *c′* support the binding of NO and CO to opposite sides of the heme: Implications for ligand discrimination in heme-based sensors, *Biochemistry 40*, 4115−4122.
34. Andrew, C. R., George, S. J., Lawson, D. M., and Eady, R. R. (2002) Six- to five-coordinate heme-nitrosyl conversion in cytochrome *c′* and its relevance to guanylate cyclase, *Biochemistry 41*, 2353−2360.
35. Othman, S., Richaud, P., Verméglio, A., and Desbois, A. (1996) Evidence for a proximal histidine interaction in the structure of cytochromes *c′* in solution: A resonance Raman study, *Biochemistry 35*, 9224−9234.
36. Kitagawa, T., Nagai, K., and Tsubaki, M. (1979) Assignment of the iron-nitrogen (His F8) stretching band in the resonance raman spectra of deoxymyoglobin, *FEBS Lett. 104*, 376−378.
37. Nagai, K., and Kitagawa, T. (1980) Differences in iron(II)-Ne-(His-F8) stretching frequencies between deoxyhemoglobins in the two alternative quaternary structures, *Proc. Natl. Acad. Sci. U.S.A. 77*, 2033−2037.
38. Teraoka, J., and Kitagawa, T. (1981) Structural implication of the heme-linked ionization of horseradish peroxidase probed by the iron-histidine stretching Raman line, *J. Biol. Chem. 256*, 3969−3977.

39. Wolff, N., Deniau, C., Letoffe, S., Simenel, C., Kumar, V., Stojiljkovic, I., Wandersman, C., Delepierre, M., and Lecroisey, A. (2002) Histidine pK_a shifts and changes of tautomeric states induced by the binding of gallium-protoporphyrin IX in the hemophore $HasA_{SM}$, *Protein Sci. 11*, 757−765.
40. Li, X. Y., and Spiro, T. G. (1988) Is bound carbonyl linear or bent in heme proteins? Evidence from resonance Raman and infrared spectroscopic data, *J. Am. Chem. Soc. 110*, 6024−6033.
41. Smulevich, G., Mauro, J. M., Fishel, L. A., English, A. M., Kraut, J., and Spiro, T. G. (1988) Cytochrome *c* peroxidase mutant active site structures probed by resonance Raman and infrared signatures of the CO adducts, *Biochemistry 27*, 5486−5492.
42. Tsubaki, M., Srivastava, R. B., and Yu, N. T. (1982) Resonance Raman investigation of carbon monoxide bonding in (carbon monoxy)hemoglobin and -myoglobin: Detection of iron-carbon monoxide stretching and iron-carbon-oxygen bending vibrations and influence of the quaternary structure change, *Biochemistry 21*, 1132−1140.
43. Takahashi, S., Wang, J., Rousseau, D. L., Ishikawa, K., Yoshida, T., Takeuchi, N., and Ikeda-Saito, M. (1994) Heme-heme oxygenase complex: Structure and properties of the catalytic site from resonance Raman scattering, *Biochemistry 33*, 5531−5538.
44. Pal, B., and Kitagawa, T. (2005) Interactions of soluble guanylate cyclase with diatomics as probed by resonance Raman spectroscopy, *J. Inorg. Biochem. 99*, 267−279.
45. Aono, S., Kato, T., Matsuki, M., Nakajima, H., Ohta, T., Uchida, T., and Kitagawa, T. (2002) Resonance Raman and ligand binding studies of the oxygen-sensing signal transducer protein HemAT from *Bacillus subtilis*, *J. Biol. Chem. 277*, 13528−13538.
46. Peterson, E. S., Friedman, J. M., Chien, E. Y. T., and Sligar, S. G. (1998) Functional implications of the proximal hydrogen-bonding network in myoglobin: A resonance Raman and kinetic study of Leu89, Ser92, His97, and F-helix swap mutants, *Biochemistry 37*, 12301−12319.
47. Wang, J., Takahashi, S., Hosler, J. P., Mitchell, D. M., Ferguson-Miller, S., Gennis, R. B., and Rousseau, D. L. (1995) Two conformations of the catalytic site in the aa_3-type cytochrome *c* oxidase from *Rhodobacter sphaeroides*, *Biochemistry 34*, 9819−9825.
48. Das, T. K., Tomson, F. L., Gennis, R. B., Gordon, M., and Rousseau, D. L. (2001) pH-Dependent structural changes at the heme-copper binuclear center of cytochrome *c* oxidase, *Biophys. J. 80*, 2039−2045.
49. Argade, P. V., Ching, Y. C., and Rousseau, D. L. (1984) Cytochrome a3 structure in carbon monoxide-bound cytochrome oxidase, *Science (Washington, DC, U.S.) 225*, 329−331.
50. Uno, T., Mogi, T., Tsubaki, M., Nishimura, Y., and Anraku, Y. (1994) Resonance Raman and Fourier transform infrared studies on the subunit I histidine mutants of the cytochrome *b*o complex in *Escherichia coli*. Molecular structure of redox metal centers, *J. Biol. Chem. 269*, 11912−11920.
51. Sato, E., Sagami, I., Uchida, T., Sato, A., Kitagawa, T., Igarashi, J., and Shimizu, T. (2004) SOUL in mouse eyes is a new hexameric heme-binding protein with characteristic optical absorption, resonance Raman spectral, and heme-binding properties, *Biochemistry 43*, 14189−14198.
52. Wardell, M., Wang, Z., Ho, J. X., Robert, J., Ruker, F., Ruble, J., and Carter, D. C. (2002) The atomic structure of human methemalbumin at 1.9 Å, *Biochem. Biophys. Res. Commun. 291*, 813−819.
53. Liu, Y., Moënne-Loccoz, P., Hildebrand, D. P., Wilks, A., Loehr, T. M., Mauk, A. G., and Ortiz de Montellano, P. R. (1999) Replacement of the proximal histidine iron ligand by a cysteine or tyrosine converts heme oxygenase to an oxidase, *Biochemistry 38*, 3733−3743.
54. Ye, X., Yu, A., Georgiev, G. Y., Gruia, F., Ionascu, D., Cao, W., Sage, J. T., and Champion, P. M. (2005) CO rebinding to protoheme: Investigations of the proximal and distal contributions to the geminate rebinding barrier, *J. Am. Chem. Soc. 127*, 5854−5861.
55. Mate, M. J., Ortiz-Lombardia, M., Marina, A., and Fita, I. (1999) Crystallization and preliminary structural results of catalase from human erythrocytes, *Acta Crystallogr., Sect. D: Biol. Crystallogr. 55*, 1066−1068.
56. Putnam, C. D., Arvai, A. S., Bourne, Y., and Tainer, J. A. (2000) Active and inhibited human catalase structures: Ligand and NADPH binding and catalytic mechanism, *J. Mol. Biol. 296*, 295−309.
57. Lawson, D. M., Stevenson, C. E. M., Andrew, C. R., and Eady, R. R. (2000) Unprecedented proximal binding of nitric oxide to heme: Implications for guanylate cyclase, *EMBO J. 19*, 5661−5671.
58. Andrew, C. R., Rodgers, K. R., and Eady, R. R. (2003) A novel kinetic trap for NO release from cytochrome *c′*: A possible mechanism for NO release from activated soluble guanylate cyclase, *J. Am. Chem. Soc. 125*, 9548−9549.
59. Caillet-Saguy, C., Delepierre, M., Lecroisey, A., Bertini, I., Piccioli, M., and Turano, P. (2006) Direct-detected ^{13}C NMR to investigate the iron(III) h emophore HasA, *J. Am. Chem. Soc. 128*, 150−158.
60. Izadi-Pruneyre, N., Huché, F., Lukat-Rodgers, G., Lecroisey, A., Gilli, R., Rodgers, K. R., Wandersman, C., and Delepelaire, P. (2006) Protein-protein interaction drives heme transfer from a high to a lower affinity binding site, *J. Biol. Chem. 281*, 25541−25550.
61. Couture, M., Das, T. K., Lee, H. C., Peisach, J., Rousseau, D. L., Wittenberg, B. A., Wittenberg, J. B., and Guertin, M. (1999) Chlamydomonas chloroplast ferrous hemoglobin. Heme pocket structure and reactions with ligands, *J. Biol. Chem. 274*, 6898−6910.

BI7019518